System validation of CO_2-laser-based phase contrast imaging on HL-2A tokamak

Yi Yu (余 羿)[1], Shaobo Gong (龚少博)[1,2], Min Xu (许 敏)[2,*], Boda Yuan (袁博达)[1,2], Yifan Wu (吴一帆)[1,2], Lin Nie (聂 林)[2], Rui Ke (柯 锐)[2], Minyou Ye (叶民友)[1], and Xuru Duan (段旭如)[2]

[1]*School of Physics, University of Science and Technology of China, Hefei 230026, China*
[2]*Southwestern Institute of Physics, Chengdu 610041, China*
**Corresponding author: minxu@swip.ac.cn*

Received June 20, 2018; accepted November 1, 2018; posted online November 29, 2018

System validation and density fluctuation calibration of phase contrast imaging (PCI) on an HL-2A tokamak are presented. Signals from different channels show not only a pronounced modulation of an incident laser beam induced by a sound wave, but also an excellent magnification and low image distortion of optics. The frequency-wavenumber spectrum is achieved by using two-dimensional Fourier transform of time series signals. The conversion coefficient between detected signal amplitude and chord integral plasma density fluctuation is $2.35 \times 10^{13}\,\mathrm{m^{-2}/mV}$, which promises a suitable signal level at the order of volts of the PCI in typical HL-2A discharges.

OCIS codes: 120.5050, 150.1488, 350.5400, 120.5060, 120.1880.
doi: 10.3788/COL201816.121201.

Not only the intensity, but also the phase of a laser beam changes when the beam passes through a medium[1,2]. Phase contrast, which now works as one of the main techniques in scientific research, such as the phase contrast microscope, is used to detect this phase change to measure the medium density. The first application of this technique in plasma science is phase contrast imaging (PCI) invented by H. Weison in a TCA tokamak to diagnose plasma density fluctuation[3]. It can greatly enhance the signal intensity contrasting the unscattered and scattered laser beams modulated by turbulent tokamak plasma by means of delaying the phase of the unscattered laser beam by $\pi/2$. The key element to introduce this phase shift is the phase plate, whose surface is coated except for a strip groove right in the middle. The special design causes the optical path difference between the unscattered and scattered laser beams and, as a result, introduces a $\pi/2$ phase shift. In the last decade, the PCI diagnostic has been developed on many large tokamaks[4–7] and other magnetic confinement devices[8] because of its broad diagnosing performance in the wavenumber domain and its high temporal resolution.

Recently, a PCI diagnostic based on a CO_2 laser has been built on an HL-2A tokamak[7]. To get the frequency-wavenumber spectrum of plasma density fluctuation, testing experiments have been done for system validation. In this article, we present optical and detecting validation of PCI, together with absolute numerical calibration of plasma density fluctuation, according to HL-2A discharging conditions.

PCI diagnostics on an HL-2A tokamak can diagnose plasma density fluctuation with a reliable maximal wavenumber range from 2 to 15 $\mathrm{cm^{-1}}$, taking into account the scintillation effect, a wavenumber resolution of 2 $\mathrm{cm^{-1}}$, and a temporal resolution of 2 μs. A 10.6 μm CO_2 laser with a maximum output power of 100 W is used as an incident beam probe. The diameter of the laser beam is expanded from 2 to 30 mm, limited by the 35 mm inner diameter of the vertical viewing windows. The diagnosed plasma is also restricted in a radial area of $0.625 < \rho = r/a < 0.7$, where $a = 0.4$ m is the minor radius of the HL-2A tokamak.

For a phase contrast system, the phase plate is the key element. A ZnSe phase plate is gold coated on the surface, leaving a 0.88 mm width rectangular groove in the center. The coating depth is 1.325 μm, which is one-eighth of the laser wavelength for contrast. Lens groups, reflecting mirrors, concave mirrors, and off-axis parabolic mirrors are also used in the optical path. A detailed optical design can be consulted in Ref. [9].

To achieve the frequency-wavenumber spectrum of turbulence, which can be calculated by Eq. (1) in the following paragraph, a 32 channel one-dimensional line detector array is developed for PCI diagnostics. Model MCT-3200, a kind of photoconductive HgCdTe (MCT) detector, is chosen as the detection element for its promised over 90% high-quality detection efficiency for infrared light with a certain wavelength of 10.6 μm. The size of every MCT element is 0.2 mm × 1.0 mm with a 0.05 mm gap between each. Adjustable pre-amplifiers are also used to enhance the gain. The electrical bandwidth can be internally set from 2 kHz to 5 MHz with different gain values.

Frequency-wavenumber spectrum $S(k, f)$ is the main description of turbulence frequency f and wavenumber k. The method for PCI to achieve a frequency-wavenumber spectrum of turbulence is a two-dimensional Fourier transform of time series signals, which are diagnosed by

simultaneous spatial multi-point measurement. As shown in Eq. (1),

$$S(k_p, f) = \left| \frac{1}{\sqrt{\Delta t}} \frac{1}{\sqrt{\Delta R}} \int_{R_1}^{R_N} \left[\int_{t_1}^{t_2} I(R,t) e^{-i2\pi f t} \mathrm{d}t \right] e^{ik_p R} \mathrm{d}R \right|^2, \tag{1}$$

where ΔR is the distance between the detectors, $\Delta t = t_2 - t_1$ is the integral time, I is signal intensity at time t, and N is the number of detection elements. Another simplified method is invented by Iwanma *et al.*[10] and Beall *et al.*[11], in which only two detector elements located closely enough are needed. In this article, the method based on Eq. (1) is used to achieve $S(k, f)$. Iwanma's simplified method shows no obvious differences in most of $S(k, f)$ calculations, but it does not work well in some specified circumstances, which will be discussed later.

The response of the PCI is gauged by standard sound waves with known frequencies in the air. The laser beam can be effectively modulated not only by turbulent plasma waves but also by pressure variation in the air generated by sound waves. A loudspeaker (model L400) is chosen as the source to launch spherical sound waves propagating across the laser beam, as shown in Fig. 1. The L400 is an ultrasound loudspeaker with a built-in amplifier. The typical frequency response extends from 10 to 110 kHz.

The CO_2 laser beam is firstly detected by the 32 channel detector array without any sound wave modulation. These tests are repeated for many times. The signals caught by two of these detection elements in four of these independent tests (data 1–data 4) are shown by color lines in Figs. 2(a) and 2(b). One can clearly see that in either of these two figures, the signal intensities are different in these four independent tests, although the same CO_2 laser is used. It indicates that the laser works stably in a certain shot but is probably not in the same working state in independent shots after restarting. For example, the absolute output power and laser noise may be different. The instability of the laser is one of the most serious problems, which is always hard to be solved, for PCI and similar laser-based diagnostics in plasmas[12]. The laser will introduce a characteristic frequency noise due to the temperature instability. Fortunately, for this PCI diagnostic, what we want to catch is the fluctuation of the turbulence,

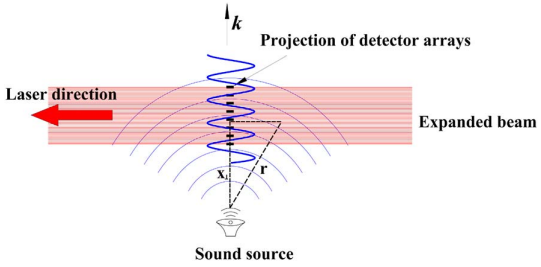

Fig. 1. PCI calibration using sound waves launched by a loudspeaker.

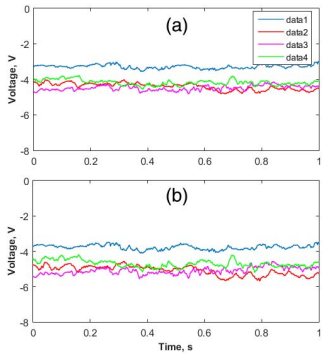

Fig. 2. Signals caught by two detection channels in four independent tests.

or, in other words, the fluctuation of the detected signals. This means that the detected signals in every detection channel are reliable if we keep the output of the laser stable in a single shot, although the laser may change somewhat its working state after restarting. The way to solve this problem for PCI is by keeping the laser working during the whole discharging campaign of HL-2A and recording the intensity of the laser as a reference signal before experiments. By the way, a much more stable laser is under construction and will work as a substitute for the old one in the near future. Another thing to be noted here is that the magnifications of the detector pre-amplifiers are not the same, comparing the intensity of the four signal series in Figs. 2(a) and 2(b). This means that the magnifications of all of these 32 pre-amplifiers are also needed to be carefully calibrated. We can draw similar conclusions by examining the signals in other tests or in other detection channels, which are not shown here just for simplicity.

To check responses of PCI under different fluctuation circumstances, sound waves with different frequencies from the loudspeaker are used to modulate the laser beam. The frequency spectra of signals from ten of the detecting channels, labeled Ch1, Ch3, etc., in the test with a 20 kHz sound wave modulation are shown in Fig. 3 by color lines. The pronounced peak of every line at the frequency of 20 kHz shows that the sound wave does modulate the laser beam, and the modulation of the laser beam by sound

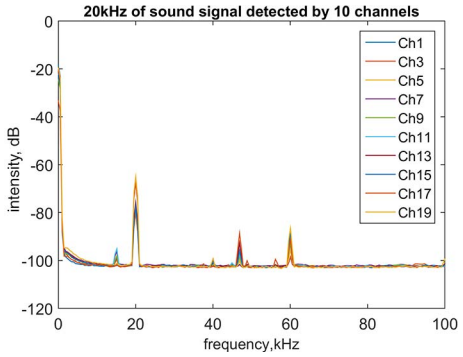

Fig. 3. Power spectra of detected signals in different channels with a 20 kHz sound wave modulation.

wave can be successfully detected by the detector array without much signal distortion. The tiny peaks at 15 kHz and the multi-frequency peaks may come from the imperfection and nonlinear harmonic components of the loudspeaker. The peak amplitudes at 20 kHz of these ten channels show obvious differences, indicating the necessity of pre-amplifier calibration.

In Fig. 4, color lines show the frequency spectra of signals from Ch9 in nine independent tests with increasing sound wave frequencies of 10, 15, 20, 30, 40, 50, 60, 70, and 80 kHz, respectively. Modulation tests with higher frequencies are not done because of the limitation of the bandwidth of the loudspeaker, which brings an output decrease as frequency increases. Pronounced peaks corresponding to the above frequencies can be obviously observed, as are expected, showing the reliability of this kind of calibration in a wide wavenumber range.

Raw signals from consecutive detection channels with a modulating sound wave frequency of 20 kHz are shown in Fig. 5. The vertical ordinate is just the number of the channels without any quantitative significance. The amplitudes of the curves show relative intensities of signals. The sampling rate of the data acquisition system is 1 MHz, and the total sampling time is 1 s. One can clearly see the low-frequency modulation (∼20 Hz) by the unstable laser output. Although a filter can be used to remove the low-frequency part at data processing, the modulation will increase the quantization noise. Obviously again, the uncalibrated magnifications of pre-amplifiers significantly make things worse by muddling the relative intensities among these detected signals. As a result, one cannot achieve a frequency-wavenumber spectrum.

A 15–25 kHz band-pass filter is used for these detected raw signals to filter out the unwanted low-frequency laser modulation. The absolute calibration of the MCT detector line array with pre-amplifiers is done by a moderate-temperature blackbody furnace modeled as R976-550. Located at a certain distance away from the furnace, which radiates a line at a fixed temperature of 200°C, the 32 detecting channels are absolutely calibrated one by one. After these processes, the signals from those channels in Fig. 5 are reworked. The time slices of signals are locally zoomed in to show the signals more clearly in Fig. 6 as solid colorful curves. It is obvious that there are three different parts in this figure, labeled as Ch group I, Ch group II, and Ch* just for convenience. In Ch group II, an observable similar phase shift exists between two nearby channels. This phase shift comes from the sound wave propagation from one channel to the next, as was shown in Fig. 1. The same conclusion can be drawn in Ch group I. An extraordinary curve Ch* (dark green solid curve) disturbs the ordered arrangement of curves, which shows obviously different phase shifts to nearby channels. Just for comparison, an imaginary dark red dash curve is drawn, showing the location where the Ch* curve should be if it keeps the same phase shift as in Ch group II. To find out the reason for this disorder, the phase shifts ϕ between adjacent detection elements normalized by $\pi/2$ are drawn in Fig. 7. All of the phase shifts are located near an averaged value of $\phi_{\text{aver}} = 0.21$ (red horizontal line), except for extraordinary values of $\phi^*_{1,2,3} \sim 1$. Those extraordinary values fit the wanted $\pi/2$ phase shift of a PCI system, as was discussed in the introduction section, subtracting the phase shift caused by the distance between two adjacent detection elements. It means that the laser detected by this detection element is reflected by the critical area between the groove and coating of the phase plate. This extraordinary Ch* curve only shows that the phase plate and optical path meet the requirements of phase delay for a PCI diagnostic.

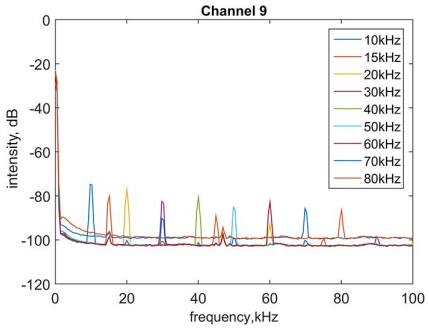

Fig. 4. Power spectra of detected signals with different sound wave modulations in Ch9.

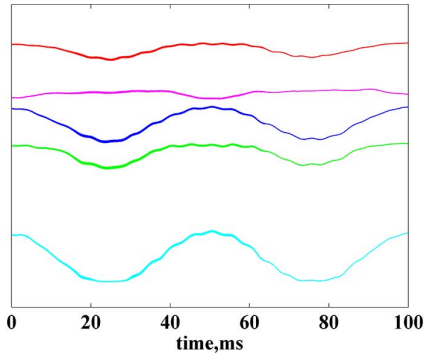

Fig. 5. Raw signals from five detecting channels with a modulating sound wave frequency of 20 kHz.

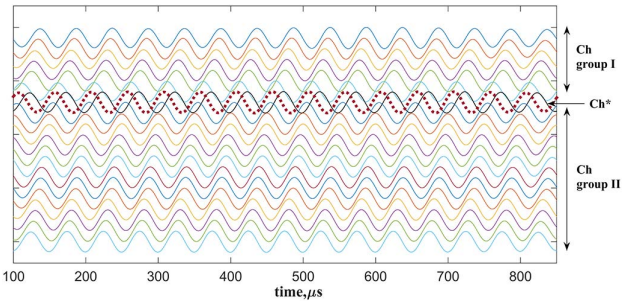

Fig. 6. Time slices of signals from detecting channels after filtering and absolute magnitude calibration.

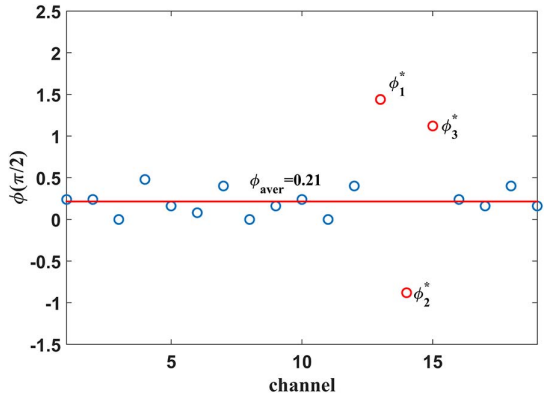

Fig. 7. Phase shifts between nearby channels.

The wavenumber k_{theory} can be calculated by $k_{\text{theory}} = 2\pi F_s / C_s$, where F_s is the frequency of the sound wave, and C_s is the sound speed. In the circumstance of Fig. 6, $F_s = 20$ kHz and $C_s = 344$ m/s at the room temperature of 22°C in the HL-2A experimental hall. So, $k_{\text{theory}} = 3.65\,\text{cm}^{-1}$. The experimentally measured frequency-wavenumber spectrum by PCI diagnostics is shown in Fig. 8, calculated by means of Eq. (1). The slope of the black line shows the constant propagation speed of the sound wave. One can clearly seen the pronounced peak at ($k_{\text{PCI}} = 3.5\,\text{cm}^{-1}$ and $f = 20$ kHz). $k_{\text{PCI}} \approx k_{\text{theory}}$, which means the measured data fits well with the theoretical prediction. Similar results are achieved with different sound wave frequencies, which are not shown here just for simplicity.

It is to be noted here that the two-dimensional Fourier transform of time series signals based on Eq. (1) is used here. Iwanma's simplified method does work if two of the detection elements in Ch group I or II are chosen. But, if Ch* is chosen as one of the detection elements, the calculated result is obviously thoroughly wrong. In the case of Fig. 6, the wave is simple with a constant frequency of 20 kHz. The plasma turbulence is a broad band turbulence, and its energy transfers among different turbulence components through nonlinear wave–wave

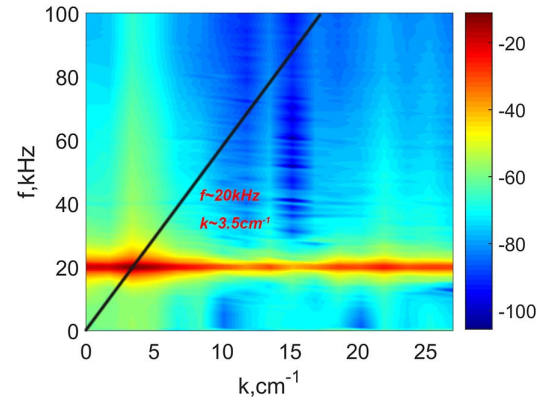

Fig. 8. Frequency-wavenumber spectrum of the signals from the 32 channel detector array after calibration.

interaction[13,14]. For PCI, which is a broad k spectrum diagnostic, Iwanma's method may bring unknown errors.

The phase shift found between two nearby signals provides a confident method for checking the magnification and distortion of the rearing optical path. The magnification coefficient M of the PCI system is designed to be 0.37[7]. The relation between M and the sound speed $C_s = 344$ m/s is given by $C_s = D/t = \Delta R/Mt$, where $D = \Delta R/\text{M}$ is the distance between two projections of two adjacent MCT elements in the sound wave modulated object plane, as shown in Fig. 1; $\Delta R = 0.2$ mm + 0.05 mm is the distance between the two corresponding MCT elements, which are located as detectors in the image plane; and $t \approx 25\,\mu\text{s}/12$ is the averaged time delay for a sound wave propagating from the projection of a certain MCT element to the one nearby in Fig. 6. Then, the experimentally measured $M = 0.35$ can be calculated. The magnification coefficient is very close to the designed one of 0.37, indicating a good technical process and the reliability of the optics.

The signal intensities are absolutely calibrated[15]. The phase fluctuation of the laser beam caused by the sound wave in the air is given by

$$\tilde{\varphi}(x_\perp) = k_0 \int \tilde{N}(x_\perp, z)\mathrm{d}z, \tag{2}$$

where $\tilde{N}$ is the fluctuation of refractive index caused by sound wave, and $x_\perp$ is the distance from the loudspeaker to the incident beam, as shown in Fig. 1. According to Gladston–Dale's law, $\tilde{N}$ is proportional to the fluctuation of air density $\tilde{\rho}$. $\tilde{N} = k_{\text{GD}}\tilde{\rho}$, where $k_{\text{GD}} = 0.22$ cm^3/g, is a constant in the mid-infrared wave range. $\tilde{\rho} = \tilde{P}/C_s^2$, where $\tilde{P}$ is the fluctuation of pressure, and $C_s = 344$ m/s is sound velocity. Equation (2) can then be rewritten as

$$\tilde{\varphi}(x_\perp) = C_0 \int \tilde{P}(x_\perp, z)\mathrm{d}z, \tag{3}$$

where constant C_0 is 1.1×10^{-11} $\frac{\text{rad}}{\mu\text{Pa}\cdot\text{cm}}$. 20 μPa is always treated as 0 dB, which is the minimal acoustic pressure that can be detected by acoustic meters. For the sound wave in the calibration, the pressure is

$$\tilde{P}(r) = r_0\tilde{P}_0 \frac{\cos(kr - \omega t)}{r}, \tag{4}$$

where $r_0\tilde{P}_0$ is a constant, and $r = \sqrt{x_\perp^2 + z^2}$ is the distance from the space point to the loudspeaker. Then, Eq. (3) can be solved theoretically[16] when $k|x_\perp| \gg 1$ and $\tilde{\varphi}(x_\perp)$ is expressed as

$$\tilde{\varphi}(x_\perp) = \left(\frac{2\pi}{k|x_\perp|}\right)^{1/2} C_0 r_0 \tilde{P}_0 \cos(k|x_\perp| - \omega t + \pi/4). \tag{5}$$

For the calibration by $f = 20$ kHz sound wave, the wavenumber is $k = 3.65$ cm^{-1}, $\tilde{P}_0 = 2 \times 10^4$ μPa, and

$r_0 = 100$ cm. At $f = 20$ kHz, the response of the loudspeaker is about 60 dB. We can achieve

$$|\tilde{\varphi}(x_\perp)| = \left(\frac{2\pi}{k|x_\perp|}\right)^{1/2} C_0 r_0 \tilde{P}_0, \tag{6}$$

where $|x_\perp| = (N_{\mathrm{Ch}} - 1)\frac{\Delta R}{M} + x_0$ is the distance between the projection of a certain detection element and the loudspeaker, N_{Ch} is sequence number of the element, $N_{\mathrm{Ch}} = 1$ means the nearest element projection to the loudspeaker, and $x_0 = 15$ cm is the distance between this projection and the loudspeaker.

For a PCI system[12], $\tilde{\varphi} = -\lambda_0 r_e \int \tilde{n}_e \mathrm{d}z$, where $r_e = e^2/4\pi\varepsilon_0 m_e c^2$ is the electron radius. We can find that

$$\int \tilde{n}_e \mathrm{d}z = \frac{C_0 r_0 \tilde{P}_0}{\lambda_0 r_e}\left[\frac{2\pi M}{k} \cdot \frac{1}{(N_{\mathrm{Ch}} - 1)\Delta R + x_0 M}\right]^{1/2}. \tag{7}$$

The light intensity measured by the detection array is shown in Fig. 9(a). The x coordinate shows the channel numbers N_{Ch}, and the y coordinate shows the output voltage u (mV) of detection elements, which is proportional to the detected light intensity. The voltage decreases as N_{Ch}, or in other words, $|x_\perp|$ increases.

The chord integral plasma density fluctuations in Eq. (7) are calculated and shown as small blue rhombuses in Fig. 9(b). All of the rhombuses are located around the red horizontal solid line of $y = 2.35 \times 10^{13}\,\mathrm{m}^{-2}/\mathrm{mV}$. This means that every 1 mV signal detected by the detection elements is the equivalent of a chord integral density fluctuation of $\tilde{n}' = 2.35 \times 10^{13}\,\mathrm{m}^{-2}$. This value is so small that a small plasma density fluctuation can cause a large enough signal in the detection element. For a typical discharging in the HL-2A tokamak, the plasma density is at the order of $n = 10^{19}\ \mathrm{m}^{-3}$, and the density fluctuation is no more than 1% at the radial location of PCI $\rho = r/a = 0.6$. For example, $\tilde{n} = 0.5 \times 1\% \times n = 5 \times 10^{16}\ \mathrm{m}^{-3}$. The chord integral length is $L = 2 \times a\sqrt{1 - (r/a)^2}$. So, it is easy to get the signal amplitude of the MCT element as $u = \tilde{n}L/\tilde{n}' \approx 1.4$ V. As is shown in Fig. 10, the raw data of the PCI detector is compatible with the predicted value, indicating the validity of sound wave calibration.

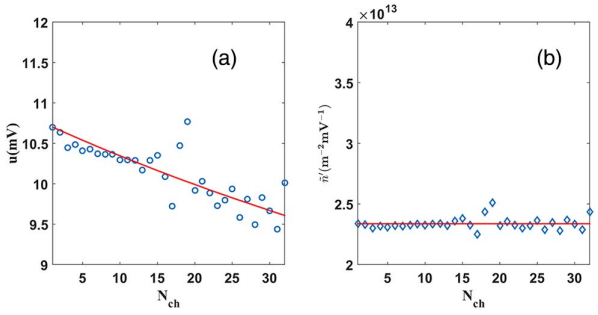

Fig. 9. (a) Voltage amplitudes in detection array; (b) conversion relations of detection array.

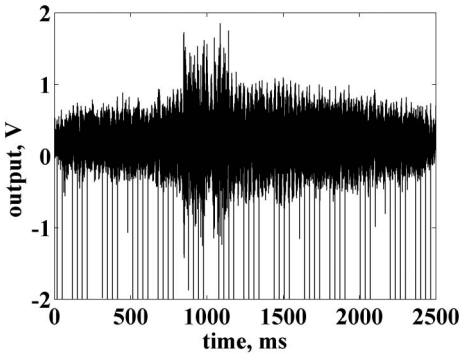

Fig. 10. Raw data of PCI detector element during plasma discharge on HL-2A tokamak; shot number, 34299.

In conclusion, PCI diagnostic based on a CO_2 laser has recently been developed on an HL-2A tokamak. The system is gauged by sound waves. The 32 channel MCT detector array with pre-amplifiers is calibrated by a moderate-temperature blackbody furnace. The signal series in different channels show not only a pronounced modulation of incident laser beam by the sound wave but also an excellent magnification and low image distortion of the optics. The frequency-wavenumber spectra derived by two-dimensional Fourier transform of time series signals caught by detection array and the comparison between different data analyses indicate a good performance of the whole PCI system and the validation of the analyzing method. Analysis of phase shift between signals shows not only the effect of wave modulation but also the effect of a phase plate. The conversion relations of all of the detection elements are tested, and a roughly coincident value of $2.35 \times 10^{13}\,\mathrm{m}^{-2}/\mathrm{mV}$ is confirmed.

This work was supported by the National Magnetic Confinement Fusion Energy Research Project (No. 2015GB120002), the National Key Research and Development Program of China (No. 2017YFE0300405), and the National Natural Science Foundation of China (Nos. 11705052, 11575055, and 11611130164).

References

1. F. Zernike, Physica **9**, 686 (1942).
2. F. Zernike, Physica **9**, 974 (1942).
3. H. Weisen, Rev. Sci. Instrum. **59**, 1544 (1988).
4. N. Tsujii, M. Porkolab, P. T. Bonoli, Y. Lin, J. C. Wright, S. J. Wukitch, E. F. Jaeger, D. L. Green, and R. W. Harvey, Phys. Plasmas **19**, 082508 (2012).
5. S. Coda, M. Porkolab, and K. H. Burrell, Phys. Lett. A **273**, 125 (2000).
6. A. Marinoni, S. Coda, R. Chavan, and G. Pochon, Rev. Sci. Instrum. **77**, 10E929 (2006).
7. S. B. Gong, Y. Yu, M. Xu, W. Jiang, W. L. Zhong, Z. B. Shi, H. J. Wang, Y. F. Wu, B. D. Yuan, T. Lan, M. Y. Ye, and X. R. Duan, Fusion Eng. Des. **123**, 802 (2017).
8. K. Tanaka, C. A. Michael, L. N. Vyachesiavov, A. L. Sanin, K. Kawahata, T. Akiyama, T. Tokuzawa, and S. Okajima, Rev. Sci. Instrum. **79**, 10E702 (2008).

9. Q. Chen, Y. Yu, S. Gong, M. Xu, T. Lan, W. Jiang, B. Yuan, Y. Wu, L. Nie, R. Ke, T. Long, D. Guo, M. Ye, and X. Duan, Plasma Sci. Tech. **19**, 125601 (2017).
10. N. Iwama, Y. Ohba, and T. Tsukishima, J. Appl. Phys. **50**, 3197 (1979).
11. J. M. Beall, Y. C. Kim, and E. J. Powers, J. Appl. Phys. **53**, 3933 (1982).
12. A. Mazurenko, *Phase Contrast Imaging on the Alcator C-Mod Tokamak* (Massachusetts Institute of Technology, 2001).
13. M. Xu, G. R. Tynan, C. Holland, Z. Yan, S. H. Muller, and J. H. Yu, Phys. Plasmas **17**, 032311 (2010).
14. M. Xu, G. R. Tynan, C. Holland, Z. Yan, S. H. Muller, and J. H. Yu, Phys. Plasmas **16**, 042312 (2009).
15. C. P. Kasten, A. E. White, and J. H. Irby, Phys. Plasmas **21**, 042305 (2014).
16. I. S. Gradshteyn and I. M. Ryzhik, *Table of Integrals, Series, and Products* (Academic Press, 1980).